CRYSTAL GROWTH & DESIGN

UCSF Library

Subscriber access provided by - Access paid by the | UCSF Library

Article

Photoisomerization and mesophase formation in azo-ionic liquids

Guillaume Bousrez, Kathrin Stappert, Magdalena Wilk-Kozubek, Brando Adranno, Hanwen
Pei, Eike T. Spielberg, Volodymyr Smetana, Anja-Verena Mudring, and Olivier Renier

Cryst. Growth Des., **Just Accepted Manuscript** • DOI: 10.1021/acs.cgd.9b01018 • Publication Date (Web): 07 Nov 2019

Downloaded from pubs.acs.org on November 8, 2019

Just Accepted

“Just Accepted” manuscripts have been peer-reviewed and accepted for publication. They are posted online prior to technical editing, formatting for publication and author proofing. The American Chemical Society provides “Just Accepted” as a service to the research community to expedite the dissemination of scientific material as soon as possible after acceptance. “Just Accepted” manuscripts appear in full in PDF format accompanied by an HTML abstract. “Just Accepted” manuscripts have been fully peer reviewed, but should not be considered the official version of record. They are citable by the Digital Object Identifier (DOI®). “Just Accepted” is an optional service offered to authors. Therefore, the “Just Accepted” Web site may not include all articles that will be published in the journal. After a manuscript is technically edited and formatted, it will be removed from the “Just Accepted” Web site and published as an ASAP article. Note that technical editing may introduce minor changes to the manuscript text and/or graphics which could affect content, and all legal disclaimers and ethical guidelines that apply to the journal pertain. ACS cannot be held responsible for errors or consequences arising from the use of information contained in these “Just Accepted” manuscripts.

is published by the American Chemical Society. 1155 Sixteenth Street N.W.,
Washington, DC 20036

Published by American Chemical Society. Copyright © American Chemical Society.
However, no copyright claim is made to original U.S. Government works, or works
produced by employees of any Commonwealth realm Crown government in the
course of their duties.

Photoisomerization and mesophase formation in azo-ionic liquids

Olivier Renier[a], Guillaume Bousrez[a], Kathrin Stappert[b], Magdalena Wilk-Kozubek[c], Brando Adranno[a], Hanwen Pei[a], Eike T. Spielberg[b], Volodymyr Smetana[a] and Anja-Verena Mudring[a,b]*

[a] Department of Materials and Environmental Chemistry, Stockholm University, Svante Arrhenius väg 16C, 10691 Stockholm, Sweden. Email: anja-verena.mudring@mmk.su.se

[b] former address: AnorganischeChemie III – Materials Engineering and Characterization, Fakultät für Chemie and Biochemie, Ruhr-Universität Bochum, 44780, Bochum, Germany.

Abstract

Ionic liquids present a versatile, highly tunable class of soft functional materials. Aside from being low melting salts, they can be endowed with additional functionalities. In N-alkylimidazolium halides, which are a prominent class of ionic liquids (ILs), the imidazolium cation was linked *via* an ether-bridge to an azobenzene unit in order to obtain photoresponsive materials through photoinduced *trans*-*cis* isomeration. The azobenzene unit, in turn, was modified with electron donating or withdrawing groups such as methyl-, *tert*-butyl-, methoxy-, *N*,*N*-dimethylamino and nitro groups to study their influence on the photoisomerization and phase behavior. Endowing the imidazolium additionally with a long alkyl chain allows the materials to potentially form liquid crystalline (LC) mesophases before melting into the isotropic liquid. All, studied compounds qualify as ionic liquids; and all, except for the nitro-compound, show the formation of smectic mesophases melting to the isotropic liquid. The compounds with the bulkiest aliphatic substituent, the *tert-butyl*, shows the lowest melting point and exhibits largest mesophase window, and shows an efficient photochemical *trans-cis* conversion (>90%). In summary, by tuning sterically and electronically the cationic part of ILs, photoswitchable room temperature liquid crystal could be developed and design guidelines for photoresponsive ionic liquids could be obtained.

1. Introduction

Ionic liquids (ILs) have received considerable attention in recent years. Their physical and chemical properties are of great interest to many research topics.[1,2] In fact, they exhibit a melting point below 100°C, are good electrical conductors and can be easily tailored to fit ones needs.[3] ILs can be used as solvents that exhibit extremely low, virtually non-existent vapor pressure, as templates for the formation of zeolites,[4] or even as reagents. Among their applications, one can find catalysis,[5–8] extraction,[9–12] and electrochemistry.[13–15] Typically, ILs have an organic cation (most commonly ammonium, sulphonium, phosphonium, imidazolium, pyridinium, picolinium, pyrrolidinium, thiazolium, oxazolium or pyrazolium) and an anionic part which is typically inorganic and weakly basic (Cl^-, Br^-, PF_6^-, etc).[16] Due to their cationic part being organic, ILs can be easily tailored by well-known substitution reactions (i.e. Suzuki, Williamson, etc…). Another interesting feature of ILs is their ability to adopt mesophases and form ionic liquid crystals (ILCs). [17] They usually are observed in an IL containing one or two anisotropically shaped ions (rod-like or disk like).[18] They exhibit order along one or more crystallographic orientations but will simultaneously demonstrate a random arrangement of cations/anions in the other directions.[19] This results most of the time in a configuration that exhibits a hydrophobic and hydrophilic part.[20] The formation of

ILCs can also be induced by the combination of rigid (i.e. aromatic) and flexible groups (i.e. aliphatic). The self-assembly and alignment of such structural features is of great influence on the formation of liquid crystalline phases. Thermotropic liquid crystals form mesophases in a certain temperature range. The thermal behavior of ILCs is influenced by the shape of the cation as well as by the shape of the anion and their interaction.[21] A change in anion can result in completely different phase transition (cold crystallization for BF_4^- *vs* only solid-solid transition with $CF_3SO_3^-$).[22]

Azobenzene based liquid crystals (Azo-ILs) have attracted considerable attention due to the possibility of using light instead of electricity to manipulate their properties.[23–25] By photoirradiation of the appropriate wavelength, it is possible to switch between the two possible isomeric states: typically, the *trans* conformation is the thermodynamically favored form which can be converted to the *cis* state by UV-light irradiation.[26] The reverse reaction (*cis* to *trans*) can be induced either thermally (Figure 1) or by photoirradiation in the visible range. However, this optical switching is only possible if the absorption spectra of the *cis* and *trans* form are sufficiently different. There are different mechanisms discussed for the isomerization process, inversion or rotation.[27,28] The reaction mechanism depends on different factors, such as solvent, pressure and substituents.[29,30]

Recently, Azo-ILs have been a splendid platform to study different applications. In fact, it has been demonstrated that they could be used as light-controlled ion transporters.[31] It has even been shown that azobenzene-imidazolium ILs can enhance the release time of drug delivery systems. [25] The photoswitchable abilities of these ILs have also shown great promise in controlling the conductivity of IL in aqueous solutions.[32] In addition, when introduced into block copolymer, azo-ILs can induce reversible changes in viscoelasticity.[33,34]

This reversible *cis-trans* photoisomerization process offers a wide range of applications[35] such as optical data storage,[36] optical switching,[37] polarization holography[38] as well as the possibility of using azo-group bearing molecules as photolabile surfactants.[39] For this reason, azobenzene based polymers and liquid crystalline polymers have been studied intensively over the last decade.[34,40,41] The study of azobenzene based ILCs has shown that the ionic character has a great influence on the mesomorphic behavior.[42] Therefore, ILs with photochromic functionalities have been developed,[43] and the photoresponsive conductivity of azobenzene based ILs has been investigated[44] together with other structural aspects. [45]

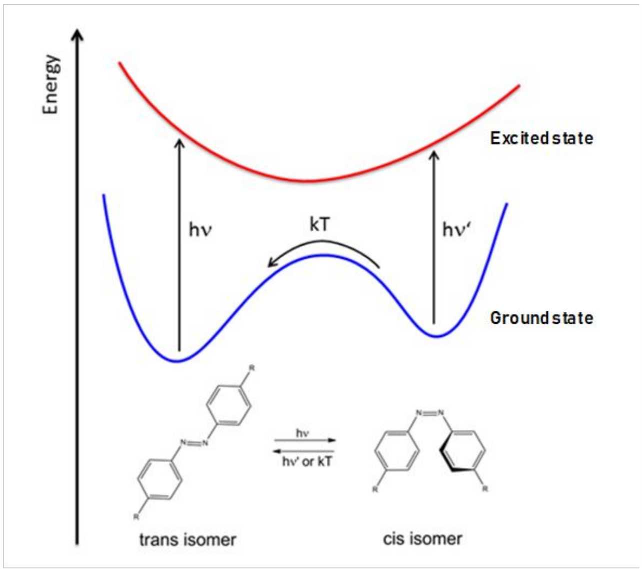

Figure 1. Energy profile for the *trans-cis* isomerization of azobenzenes.

The aim of this study is to determine the influence of different substituents at the azobenzene moiety on the efficiency of the photoinduced *trans-cis* isomerization as well as on the thermal phase behavior in order to provide improved design guidelines for the deliberate development of this interesting class of materials. To this avail, we have chosen to study imidazolium bromides, where the cation is functionalized with a dodecyl-side chain that can act as a mesogenic group and an azobenzene moiety linked *via* an ether-bridge to the cationic head group to allow for additional flexibility and varied the –R group by exploring methyl-, *tert*-butyl-, methoxy-, *N,N*-dimethylamino and nitro groups (Figure 2).

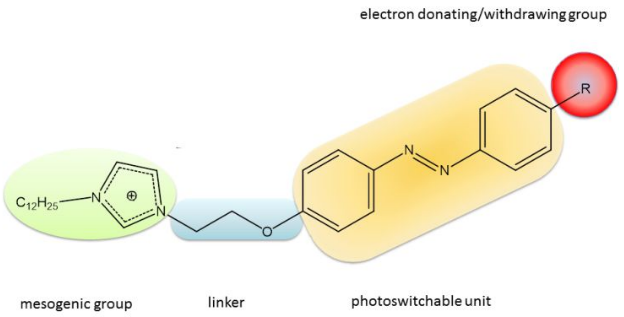

Figure 2. General structure of the studied compounds (R = Me (**1**), t-Bu (**2**), OMe (**3**), NMe_2 (**4**), NO_2 (**5**)).

2. Experimental Section

2.1. Materials

All chemicals were purchased from Sigma-Aldrich or VWR and used as received.

2.2. Synthesis

<u>Synthesis of phenyldiazenylphenol derivatives **1b-5b**</u>

Aniline derivative (**1a-5a**) (10 mmol, 1 eq.) and concentrated hydrochloric acid (37%) (2.5 mL) were dissolved in water (10 mL). $NaNO_2$ (690 mg, 10 mmol, 1 eq.) in 1.5 mL water was slowly added at 0°C. The solution was stirred during 4h. Phenol (940 mg, 10 mmol, 1 eq.), Na_2CO_3 (1,092 mg, 10.3 mmol, 1.03 eq.) and NaOH (400 mg, 10 mmol, 1 eq.) were dissolved in water (10 mL) and then added dropwise to the solution. The mixture was stirred for another 4h at room temperature. After adjusting the pH to 7 with hydrochloric acid the precipitated product was filtered off, washed with water (3 x 20 mL) and dried under vacuum at room temperature for 24h.

4-Methylphenyldiazenylphenol (**1b**)

Orange solid. ^{1}H NMR (400 MHz, $CDCl_3$, δ/ppm): 2.42 (s, 3H), 6.93 (d, J_{H-H} = 8.4 Hz, 2H), 7.29 (d, J_{H-H} = 8.0 Hz, 2H), 7.79 (d, J_{H-H} = 7.6 Hz, 2H), 7.86 (d, J_{H-H} = 8.0 Hz, 2H). ν_{max} (cm^{-1}): 3025, 2917, 2792, 1601, 1579, 1501, 1459, 1404, 1369, 1275, 1220, 1184, 1156, 1139, 1101, 1035, 1020, 938, 825, 755, 721, 705, 645, 614, 596, 545, 532, 503, 465, 423, 414.

4-Tert-butylphenyldiazenylphenol (**2b**)

Orange solid. ^{1}H NMR (400 MHz, $CDCl_3$, δ/ppm): 1.37 (s, 9H), 6.93 (d, J_{H-H} = 8.4 Hz, 2H), 7.52 (d, J_{H-H} = 8.4 Hz, 2H), 7.82 (d, J_{H-H} = 8.8 Hz, 2H), 7.85 (d, J_{H-H} = 8.4 Hz, 2H). ν_{max} (cm^{-1}): 3356, 3056, 2958, 2902, 2866, 1901, 1784, 1589, 1500, 1460, 1431, 1393, 1362, 1265, 1226, 1140, 1103, 1022, 1010, 947, 837, 789, 756, 718, 699, 632, 565, 532, 492, 450, 421.

4-Methoxyphenyldiazenylphenol (**3b**)

Orange solid. ^{1}H NMR (400 MHz, $CDCl_3$, δ/ppm): 3.88 (s, 3H), 6.93 (d, J_{H-H} = 8.4 Hz, 2H), 7.00 (d, J_{H-H} = 9.2 Hz, 2H), 7.83 (d, J_{H-H} = 8.4 Hz, 2H), 7.88 (d, J_{H-H} = 8.4 Hz, 2H). ν_{max} (cm^{-1}): 3410, 3025, 2958, 2838, 2052, 1981, 1596, 1582, 1494, 1461, 1438, 1352, 1317, 1304, 1233, 1176, 1149, 1103, 1028, 1014, 959, 945, 841, 750, 731, 645, 604, 555, 531, 504, 429, 409.

4-Dimethylaminophenyldiazenylphenol (**4b**)

Brown solid. ^{1}H NMR (400 MHz, $CDCl_3$, δ/ppm): 3.06 (s, 6H), 6.74 (d, J_{H-H} = 8.8 Hz, 2H), 6.92 (d, J_{H-H} = 8.8 Hz, 2H), 7.76 (d, J_{H-H} = 8.8 Hz, 2H), 7.82 (d, J_{H-H} = 9.2 Hz, 2H). ν_{max} (cm^{-1}): 3062, 3024, 2910, 2802, 2672, 1598, 1582, 1558, 1521, 1499, 1478, 1442, 1393, 1371, 1314, 1269, 1230, 1146, 1102, 1062, 843, 833, 818, 796, 754, 718, 646, 589, 551, 537,511, 497, 434, 413, 402.

4-Nitrophenyldiazenylphenol (**5b**)

Brown solid. ^{1}H NMR (400 MHz, $CDCl_3$, δ/ppm): 6.97 (d, J_{H-H} = 8.8 Hz, 2H), 7.93 (d, J_{H-H} = 8.8 Hz, 2H), 7.97 (d, J_{H-H} = 8.8 Hz, 2H), 8.36 (d, J_{H-H} = 8.8 Hz, 2H). ν_{max} (cm^{-1}): 3383, 3110, 1604, 1584, 1503, 1457, 1429, 1402, 1379, 1332, 1281, 1178, 1136, 1101, 1006, 859, 845, 755, 722, 685, 640, 603, 536, 510, 422, 400.

Synthesis of 1-(4-((2-bromoethyl)oxy)phenyl)-2-(phenyl)diazene derivatives **1c-5c**

A mixture of **1b-5b** (15 mmol, 1 eq.), 1,2-dibromoethane (45 mmol, 3 eq.) and K_2CO_3 (55.5 mmol, 3.7 eq.) in acetonitrile (10 mL) was heated under refluxed during 20 h. After cooling down to room temperature the suspension was poured into water and extracted with dichloromethane. The combined organic phases were dried with magnesium sulfate, filtered and the solvent was removed under vacuum. The product was dried under vacuum at room temperature for 20 hours to give an orange powder.

1-(4-((2-Bromoethyl)oxy)phenyl)-2-(4-methylphenyl)diazene (**1c**)

Orange solid. ^{1}H NMR (400 MHz, $CDCl_3$, δ/ppm): 2.43 (s, 3H), 3.68 (t, $J_{H\text{-}H}$ = 6.0 Hz, 2H), 4.37 (t, $J_{H\text{-}H}$ = 6.0 Hz, 2H), 7.02 (d, $J_{H\text{-}H}$ = 8.8 Hz, 2H), 7.30 (d, $J_{H\text{-}H}$ = 7.6 Hz, 2H), 7.80 (d, $J_{H\text{-}H}$ = 8.4 Hz, 2H), 7.91 (d, $J_{H\text{-}H}$ = 8.4 Hz, 2H). ν_{max} (cm^{-1}): 3025, 2921, 2861, 2736, 1598, 1579, 1492, 1453, 1416, 1381, 1315, 1295, 1275, 1235, 1142, 1114, 1073, 1013, 962, 880, 849, 820, 784, 745, 724, 705, 641, 633, 618, 571, 551, 528, 513, 422, 400.

1-(4-((2-Bromoethyl)oxy)phenyl)-2-(4-tert-butylphenyl)diazene (**2c**)

Orange solid. ^{1}H NMR (400 MHz, $CDCl_3$, δ/ppm): 1.37 (s, 9H), 3.68 (t, $J_{H\text{-}H}$ = 6.4 Hz, 2H), 4.38 (t, $J_{H\text{-}H}$ = 6.0 Hz, 2H), 7.02 (d, $J_{H\text{-}H}$ = 8.8 Hz, 2H), 7.52 (d, $J_{H\text{-}H}$ = 8.4 Hz, 2H), 7.83 (d, $J_{H\text{-}H}$ = 8.4 Hz, 2H), 7.92 (d, $J_{H\text{-}H}$ = 8.8 Hz, 2H). ν_{max} (cm^{-1}): 3054, 2958, 2866, 1599, 1584, 1497, 1456, 1416, 1389, 1363, 1297, 1281, 1264, 1246, 1225, 1178, 1161, 1143, 1105, 1077, 1010, 969, 943, 878, 836, 768, 720, 698, 631, 603, 568, 546, 525, 511, 468, 453, 423.

1-(4-((2-Bromoethyl)oxy)phenyl)-2-(4-methoxyphenyl)diazene (**3c**)

Orange solid. ^{1}H NMR (400 MHz, $CDCl_3$, δ/ppm): 3.67 (t, $J_{H\text{-}H}$ = 6.4 Hz, 2H), 3.89 (s, 3H), 4.37 (t, $J_{H\text{-}H}$ = 6.4 Hz, 2H), 7.01 (d, $J_{H\text{-}H}$ = 8.8 Hz, 2H), 7.01 (d, $J_{H\text{-}H}$ = 9.2 Hz, 2H), 7.89 (d, $J_{H\text{-}H}$ = 8.8 Hz, 2H), 7.89 (d, $J_{H\text{-}H}$ = 8.8 Hz, 2H). ν_{max} (cm^{-1}): 3061, 2998, 2969, 2910, 2859, 2838, 2728, 2617, 2556, 2036, 1999, 1913, 1592, 1495, 1454, 1440, 1418, 1386, 1304, 1282, 1243, 1177, 1142, 1102, 1071, 1010, 957, 877, 843, 812, 783, 744, 731, 640, 580, 548, 506, 419.

1-(4-((2-Bromoethyl)oxy)phenyl)-2-(4-dimethylaminophenyl)diazene (**4c**)

Brown solid. ^{1}H NMR (400 MHz, CDCl$_3$, δ/ppm): 3.08 (s, 6H), 3.67 (t, $J_{H\text{-}H}$ = 6.0 Hz, 2H), 4.36 (t, $J_{H\text{-}H}$ = 6.0 Hz, 2H), 6.76 (d, $J_{H\text{-}H}$ = 8.8 Hz, 2H), 6.99 (d, $J_{H\text{-}H}$ = 8.8 Hz, 2H), 7.82-7.86 (m, 4H). ν_{max} (cm^{-1}): 3068, 3029, 2854, 2795, 1676, 1594, 1513, 1495, 1442, 1403, 1356, 1308, 1223, 1168, 1146, 1059, 1011, 941, 816, 751, 730, 691, 641, 613, 575, 547, 535, 522, 417, 406.

1-(4-((2-Bromoethyl)oxy)phenyl)-2-(4-nitrophenyl)diazene (**5c**)

Brown solid. ^{1}H NMR (400 MHz, CDCl$_3$, δ/ppm): 3.69 (t, $J_{H\text{-}H}$ = 6.0 Hz, 2H), 4.41 (t, $J_{H\text{-}H}$ = 6.0 Hz, 2H), 7.06 (d, $J_{H\text{-}H}$ = 8.4 Hz, 2H), 7.97-8.00 (m, 4H), 8.37 (d, $J_{H\text{-}H}$ = 8.8 Hz, 2H). ν_{max} (cm^{-1}): 3105, 3073, 2969, 2923, 2851, 1783, 1688, 1600, 1580, 1521, 1493, 1456, 1419, 1403, 1385, 1341, 1296, 1279, 1243, 1181, 1135, 1106, 1068, 1012, 966, 920, 881, 857, 841, 816, 754, 723, 683, 636, 578, 546, 537, 510, 495, 458, 418.

Synthesis of ionic liquids **1-5**

A mixture of **1c-5c** (10 mmol, 1 eq.) and dodecylimidazole (10 mmol, 1 eq.) was heated under reflux in acetonitrile (5 mL) for three days. After cooling down the product was washed with ethyl acetate (3 x 20 mL). To obtain the precipitation of the final product the Schlenk tube is put at -80°C during one hour. The precipitate was filtered off and dried under vacuum at room temperature overnight.

We have reported on 1 previously.[45] Compound **1** in the current study corresponds to **2c** in ref 45. We have re-synthesized the material and measured additional chemical and physical properties. We have re-evaluated its crystal structure (c.f. CCDC1036110 to 1902398, no changes to the data and refinement results) to compare its structural similarities to compound **3** reported here.

1-Dodecyl-3-(2-(4-((4-methylphenyl)diazenyl)phenoxy)ethyl)-imidazolium bromide (**1**)

Orange solid. ^{1}H NMR (400 MHz, $CDCl_3$, δ/ppm): 0.82 (t, J_{H-H} = 6.4Hz, 3H), 1.17 (s, 14H), 1.25 (s, 4H), 1.84-1.85 (m, 2H), 2.37 (s, 3H), 4.25 (t, J_{H-H} = 7.2 Hz, 2H), 4.47 (t, J_{H-H} = 4.4 Hz, 2H), 4.93-4.94 (m, 2H), 6.98 (d, J_{H-H} = 8.8 Hz, 2H), 7.23 (d, J_{H-H} = 8.0 Hz, 2H), 7.37 (s, 1H), 7.72 (d, J_{H-H} = 8.0 Hz, 2H), 7.79-7.72 (m, 3H), 10.39 (s, 1H). ^{13}C NMR (100 MHz, $CDCl_3$, δ/ppm): 14.1, 21.5, 22.7, 26.3, 29.0, 29.3, 29.4, 29.5, 29.6 (2C), 30.2, 31.9, 49.4, 50.3, 66.6, 114.8 (2C), 121.6, 122.6 (2C), 123.5, 124.6 (2C), 129.7 (2C), 137.2, 141.2, 147.6, 150.6, 159.6. ν_{max} (cm^{-1}): 3168, 3168, 3133, 3089, 3063, 2951, 2923, 2867, 2848, 1599, 1583, 1570, 1498, 1474, 1462, 1411, 1377, 1359, 1312, 1297, 1241, 1222, 1190, 1152, 1113, 1102, 1055, 1042, 1017, 1006, 974, 945, 919, 919, 873, 841, 821, 805, 790, 770, 751, 726, 705, 694, 645, 634, 618, 594, 548, 534, 466, 423. ESI TOF *m/z* (positive mode) 475.4086 (calculated *m/z* = 475.3431).

1-Dodecyl-3-(2-(4-((4-tert-butylphenyl)diazenyl)phenoxy)ethyl)-imidazolium bromide (**2**)

Orange solid. ^{1}H NMR (400 MHz, $CDCl_3$, δ/ppm): 0.82 (t, J_{H-H} = 6.4 Hz, 3H), 1.17 (s, 14H), 1.25 (s, 4H), 1.31 (s, 9H), 1.83-1.85 (m, 2H), 2.44 (s, 1H), 4.25 (t, J_{H-H} = 7.2 Hz, 2H), 4.48 (t, J_{H-H} = 4.4 Hz, 2H), 4.93-4.94 (m, 2H), 6.99 (d, J_{H-H} = 8.0 Hz, 2H), 7.36 (d, J_{H-H} = 1.2 Hz, 1H), 7.46 (d, J_{H-H} = 8.4 Hz, 2H), 7.74-7.82 (m, 5H), 10.31 (s, 1H). ^{13}C NMR (100 MHz, $CDCl_3$, δ/ppm): 14.1, 22.6, 26.3, 29.0, 29.3, 29.4, 29.5, 29.6 (2C), 30.2, 31.3 (3C), 31.9, 34.9, 49.4, 50.3, 66.6, 114.8 (2C), 121.6, 122.4 (2C), 123.5, 124.6 (2C), 126.0 (2C), 137.2, 147.7, 150.5, 154.2, 159.6. ν_{max} (cm^{-1}): 3358, 3149, 3126, 3086, 3059, 2958, 2920, 2850, 1649, 1602, 1586, 1553, 1500, 1467, 1420, 1397, 1363, 1322, 1300, 1258, 1240, 1181, 1156, 1143, 1107, 1054, 1013, 951, 918, 863, 844, 807, 777, 722, 693, 659, 630, 600, 566, 535, 479, 429, 401. ESI TOF *m/z* (positive mode) 517.4017 (calculated *m/z* = 517.3901).

1-Dodecyl-3-(2-(4-((4-methoxyphenyl)diazenyl)phenoxy)ethyl)-imidazolium bromide (**3**)

Yellow solid. ^{1}H NMR (400 MHz, $CDCl_3$, δ/ppm): 0.80 (t, J_{H-H} = 6.8 Hz, 3H), 1.16 (s, 14H), 1.25 (s, 4H), 1.84-1.87 (m, 2H), 3.82 (s, 3H), 4.21 (t, J_{H-H} = 7.6 Hz, 2H), 4.45 (t, J_{H-H} = 8.4 Hz, 2H), 4.95 (t, J_{H-H} = 8.4 Hz, 2H), 6.93 (d, J_{H-H} = 7.6 Hz, 4H), 7.20 (s, 1H), 7.60 (s, 1H), 7.79 (d, J_{H-H} = 8.8 Hz, 2H), 7.81 (d, J_{H-H} = 8.8 Hz, 2H), 10.60 (s, 1H). ^{13}C NMR (100 MHz, $CDCl_3$, δ/ppm): 14.2, 22.8, 26.4, 29.1, 29.4, 29.5, 29.6, 29.7 (2C), 30.3, 32.0, 49.6, 50.5, 55.7, 66.9, 114.3 (2C), 114.8 (2C), 121.3, 123.5, 124.6 (2C), 124.6 (2C), 137.8, 147.0, 147.8, 159.3, 161.9. ν_{max} (cm^{-1}): 3169, 3134, 3087, 3061, 2947, 2923, 2864, 2849, 1599, 1583, 1570, 1500, 1474, 1463, 1422, 1413, 1382, 1371, 1359, 1315, 1298, 1238, 1223, 1178, 1151, 1108, 1057, 1040, 974, 940, 919, 873, 844, 820, 807, 770, 751, 728, 694, 643, 619, 595, 548, 528, 489, 453, 436, 411. ESI TOF *m/z* (positive mode) 491.3576 (calculated *m/z* = 491.3381).

1-Dodecyl-3-(2-(4-((4-dimethylaminophenyl)diazenyl)phenoxy)ethyl)-imidazolium bromide (**4**)

Brown solid. ^{1}H NMR (400 MHz, $CDCl_3$, δ/ppm): 0.82 (t, $J_{H\text{-}H}$ = 6.4 Hz, 3H), 1.17 (s, 14H), 1.23 (s, 4H), 1.81-1.82 (m, 2H), 3.01 (s, 6H), 4.21 (t, $J_{H\text{-}H}$ = 7.2 Hz, 2H), 4.42 (t, $J_{H\text{-}H}$ = 4.4 Hz, 2H), 4.87-4.88 (m, 2H), 6.67 (d, $J_{H\text{-}H}$ = 8.4 Hz, 2H), 6.93 (d, $J_{H\text{-}H}$ = 8.4 Hz, 2H), 7.33 (s, 1H), 7.72-7.78 (m, 5H), 10.28 (s, 1H). ^{13}C NMR (100 MHz, $CDCl_3$, δ/ppm): 14.1, 22.6, 26.2, 29.0, 29.3, 29.4, 29.5, 29.6 (2C), 31.9 (2C), 40.3 (2C), 49.4, 50.2, 66.5, 111.5 (2C), 114.8 (2C), 121.6, 123.5, 123.8 (2C), 124.6 (2C), 137.1, 143.4, 148.0, 152.2, 158.5. ν_{max} (cm^{-1}): 3357, 3133, 3035, 2922, 2851, 1898, 1671, 1597, 1584, 1561, 1511, 1497, 1466, 1449, 1449, 1405, 1353, 1322, 1293, 1228, 1164, 1150, 1101, 1054, 1005, 944, 913, 890, 833, 823, 778, 724, 686, 655, 642, 595, 548, 535, 439, 430, 405. ESI TOF *m/z* (positive mode) 504.4475 (calculated *m/z* = 504.3697).

1-Dodecyl-3-(2-(4-((4-nitrophenyl)diazenyl)phenoxy)ethyl)-imidazolium bromide (**5**)

Brown solid. ^{1}H NMR (400 MHz, $CDCl_3$, δ/ppm): 0.87 (t, $J_{H\text{-}H}$ = 7.2 Hz, 3H), 1.23 (s, 14H), 1.34 (s, 4H), 1.61 (s, 2H), 1.94 (s, 2H), 4.26 (t, $J_{H\text{-}H}$ = 7.2 Hz, 2H), 4.59 (s, 2H), 5.04 (s, 2H), 7.05 (d, $J_{H\text{-}H}$ = 8.8 Hz, 2H), 7.18 (s, 1H), 7.53 (s, 1H), 7.97 (d, $J_{H\text{-}H}$ = 8.4 Hz, 2H), 7.99 (d, $J_{H\text{-}H}$ = 8.4 Hz, 2H), 8.37 (d, $J_{H\text{-}H}$ = 8.4 Hz, 2H), 10.80 (s, 1H). ^{13}C NMR (100 MHz, $CDCl_3$, δ/ppm): 14.2, 22.8, 26.4, 29.1, 29.4, 29.5, 29.6, 29.7 (2C), 30.3, 32.0, 49.6, 50.6, 67.0, 115.1 (2C), 121.4, 123.3 (2C), 123.6, 124.8 (2C), 125.7 (2C), 137.6, 147.5, 148.4, 155.8, 161.0. ν_{max} (cm^{-1}): 3382, 3056, 2921, 2850, 2446, 2090, 1926, 1597, 1544, 1519, 1503, 1462, 1403, 1340, 1300, 1251, 1163, 1137, 1106, 1051, 1030, 1005, 914, 859, 837, 777, 754, 736, 721, 684, 635, 585, 542, 511, 491, 442. ESI TOF *m/z* (positive mode) 506.3727 (calculated *m/z* = 506.3126).

Synthesis of dodecylimidazole (**6**)

Potassium hydroxide (100 mmol, 2 eq) was added to a solution of imidazole (50 mmol, 1 eq) in DMSO (20 mL) and the mixture was stirred for 30 min at room temperature. Dodecyliodide (50 mmol, 1 eq) was added portion-wise under vigorous stirring in a water bath and the stirring was continued overnight. The mixture was then quenched with water (200 mL) and extracted with diethyl ether (3 x 25 mL). The combined extracts were washed with water, dried over anhydrous magnesium sulphate and the solvent was evaporated off under reduced pressure.

Orange oil. ^{1}H NMR (400 MHz, $CDCl_3$, δ/ppm): 0.82 (t, $J_{H\text{-}H}$ = 7.2 Hz, 3H), 1.19 (s, 18H), 1.67-1.72 (m, 2H), 3.84 (t, $J_{H\text{-}H}$ = 7.2 Hz, 2H), 6.83 (s, 1H), 6.96 (s, 1H), 7.37 (s, 1H). ν_{max} (cm^{-1}): 3106, 2922, 2852, 1678, 1568, 1506, 1465, 1376, 1282, 1228, 1163, 1108, 1076, 1031, 907, 807, 725, 663, 624.

2.3. Instrumentation

Differential scanning calorimetry (DSC) was performed with a computer-controlled Phoenix DSC 204 F1 thermal analyzer (Netzsch, Selb, Germany). Measurements were carried out at a heating rate of 5°C/min in sealed aluminum crucible with an argon flow rate of 40 mL/min. The samples were placed in aluminum pans which were cold-sealed. Given temperatures correspond to the maximum of the respective thermal process.

Thermogravimetric Analysis (TG) was performed with a TG 449 F3 Jupiter (Netzsch, Selb, Germany). Measurements were carried out in aluminum oxide crucibles with a heating rate of 10°C/min and nitrogen as purge gas.

The infrared spectroscopy (IR) was conducted with a Bruker Alpha-P ATR-spectrometer (Karlsruhe, Germany) in attenuated total reflection configuration. The data evaluation was carried out with the program OPUS.

^{1}H and ^{13}C NMR spectra were recorded at room temperature in $CDCl_3$ or DMSO on a Bruker 400 MHz spectrometer equipped with a BBO probe. Chemical shifts are reported in delta (δ) units, expressed in parts per million (ppm). The following abbreviations used for the observed multiplicities: s (singlet), d (doublet), t (triplet), q (quartet), m (multiplet for unresolved lines). ^{1}H NMR chemical shifts were referenced to the residual solvent signal for $CDCl_3$ (7.26 ppm) and ^{13}C NMR chemical shifts were referenced to the solvent signal of $CDCl_3$ (77.16 ppm).

The ESI mass spectrometry was conducted with A SYNAPT G2-S HDMS Q-ToF Mass Spectrometer (Waters, Manchester, UK) in positive and negative ion mode.

Optical analyses were made by heated-stage polarized optical microscopy (POM) with an Axio Imager A1 microscope (Carl Zeiss MicroImaging GmbH,Göttingen, D) equipped with a hot stage, THMS600 (Linkam Scientific Instruments Ltd, Surrey, UK), and Linkam TMS 94 temperature controller (Linkam Scientific Instruments Ltd, Surrey, UK). Images were recorded at a magnification of 100× as a video with a digital camera during heating and cooling the sample which was places between two cover slips. Heating and cooling rates were 5°C/min.

UV-Vis absorption spectra of methanolic solutions of **1–5** were recorded on an Agilent Technologies Cary 50 UV-Vis spectrophotometer using 1 cm light-path quartz cuvettes. UV-Vis absorption spectra of neat samples, which were molten before the measurement, were recorded on an Agilent Technologies Cary 5000 UV-Vis-NIR spectrophotometer equipped with a Praying Mantis diffuse reflectance accessory. The irradiation of the samples was conducted in a box equipped with an open UV lamp installed in the upper part of the hood (CAMAG). For irradiation, the samples were placed in the box and exposed to UV light of 366 nm for 10 min. UV-Vis measurements and UV irradiation were performed at room temperature.

Crystals of compounds **1–3** were obtained from recrystallization of the corresponding samples in dichloromethane/acetonitrile solution. Compound had been studied by us previously.[45] We did the reinvestigation of the crystal structure as compound 3 is isostructural with compound 1 and we discuss their similarities and differences." Data sets were collected using various single-crystal X-Ray diffractometer a Stoe IPDS-I (Mo K_α, at 100 K), a Bruker D8 Venture (Mo K_α, at 293 K) and an Agilent SuperNova (Cu K_α, at 107 K). Crystal structure solution by direct methods using SIR 92[46] or SHELXT[47] yielded the heavy atom positions. Refinement with SHELXL-97[48] allowed for the localization of the remaining atom positions. Hydrogen atoms were added and treated with the riding atom mode. Data reduction was performed with the program package X-Red[49] or SAINT[50] and absorption corrections were carried out with the programs X-Shape[51] or SADABS.[52] To illustrate the crystal structures, the program Diamond[53] was used.

Theoretical calculations based on the DFT (density functional theory) method are utilized to investigate the mechanism of photoisomerization of compounds **1-5**. All of the calculations are performed by the Gaussian09 program package.[54] Ground state geometry optimization of azobenzene compounds and the calculation of HOMO-LUMO gap are done using B3PW91 functional[55] and 6-311++G(d,p) basis set in gas phase. Note that, polarization functions improve the description of molecular geometries. The diffuse function are represented by “+” sign, which considers the effect of electrons far away from the nucleus. The polarizable continuum model (PCM) is utilized to evaluate the bulk solvent effects on the absorption spectra.[56]

3. Results and Discussion

3.1. Synthesis

In a first step an azo-coupling between a substituted aniline and phenol (Scheme 1) was carried out, followed by a Williamson ether synthesis with 1,2-dibromoethane. Finally, conversion to the bromide salt was achieved by alkylation of dodecylimidazole.

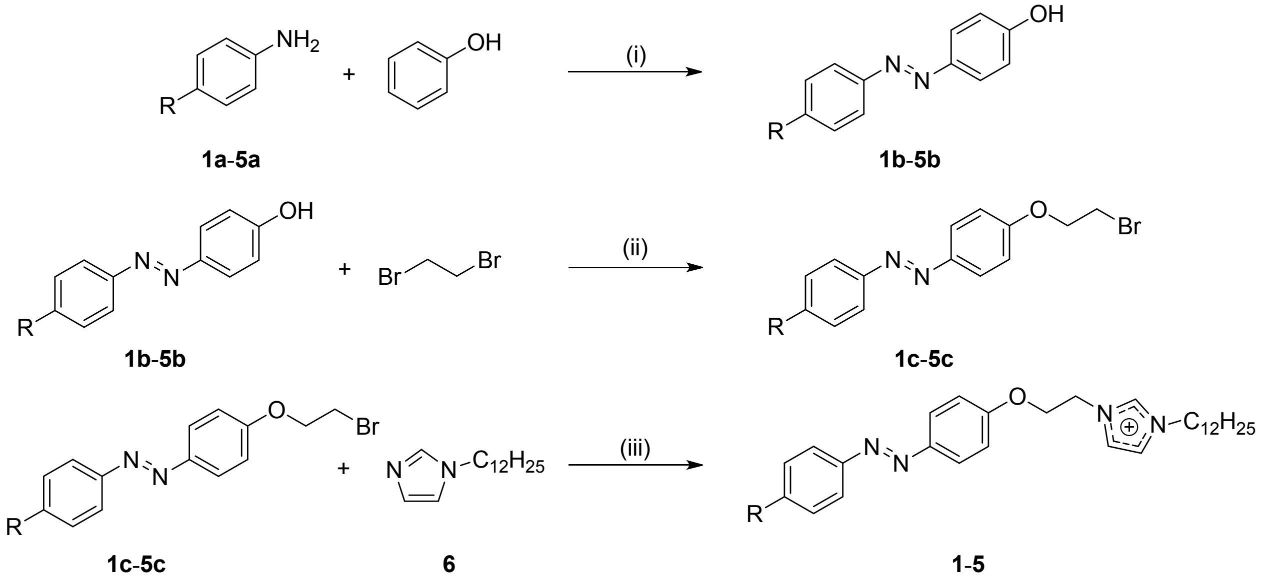

Scheme 1. Synthesis of compounds **1–5**. i) $NaNO_2$, NaOH, Na_2CO_3, HCl, H_2O, r.t., 4h; ii) K_2CO_3, CH_3CN, reflux, 20h; iii) CH_3CN, reflux, 72h.

3.2. Structure Analysis

Single crystals of compounds **1** and **3** could be grown from a dichloromethane/acetonitrile solution. The hemihydrate of **2** could be obtained by isothermal evaporation of acetonitrile solution at ambient conditions. Despite intense trying various solvents and solvent combinations, crystals of **4** and **5** with sufficient quality for X-ray structure analysis could not be obtained.

Compounds **1** and **3** crystallize in the triclinic space group $P\overline{1}$ and are isostructural. The alkyl chain and the azobenzene unit planes are oriented virtually perpendicular (65–75°) to the imidazolium ring but parallel to each other, resembling the letter "U" from a certain perspective (Figure 3 top). Nevertheless, these chains (the arms of the molecule) are entirely orthogonal in the projection on the *ac* plane, resembling the letter "V" (Figure 3 bottom). Expectedly, the azobenzene unit adopts a *trans* conformation in all crystal structures. The organic cations form bilayers with head-to-head arrangement. The latter connects through offset head-to-head $\pi\cdots\pi$ interactions ($d_{Cg\cdots Cg}$ = 3.91 Å, slippage = 1.68 Å) and weak and strongly delocalized C−H···Br interactions ($d_{H\cdots Br}$ above 2.9 Å). Each Br^- anion is hypothetically bound to six large organic cations, mostly through aromatic ring H atoms. Different arms of the neighboring intralayer cations connect through rather strong C−H···π interactions ($d_{H\cdots Cg}$ = 2.93 Å for **1** and $d_{H\cdots Cg}$ = 2.84 Å for **3**) forming a zigzag. The interlayer contacts are limited to the weak C−H···π ($d_{H\cdots Cg}$ = 4.08 Å) and weak electrostatic interactions between the terminal $-CH_3$ groups of the alkyl chains and the $-CH_3$ groups of the R substituents. It is interesting that in the case of $-OCH_3$ substituent the distances between the closest $-CH_3$ groups slightly increase but due to the presence of the oxygen atom one $-CH_3$ group moves closer to the arm of the neighboring organic cation adding one more comparable interaction.

The crystal structure of **2**·0.5 H_2O (Figure 4) exhibits similar bilayers though with different internal ordering due to different conformation of the cations and enhanced bonding between two parts of the bilayer perhaps due to formation of the solvate. In contrast to **1** and **3**, the alkyl chain and the azobenzene unit planes form a smaller angle (45−50°) with the imidazolium ring and, instead of parallel stacking, build zigzag chains along the *a* axis. Within one layer cations alternate approximately along [011] being orthogonal to each other. Head-to-head π···π interactions between the imidazolium rings are shorter ($d_{Cg\cdots Cg}$ = 3.52 Å, slippage = 0.79 Å), while no C−H···π interactions are observed between the arms of different molecules. Instead, strong C−H···π interactions ($d_{H\cdots Cg}$ = 3.56 Å) appeared between the arms of the same molecule connecting the second benzene ring with the terminal -C_2H_5 group and stabilizing the “U” shape. The interlayer contacts are now represented by a more extended network of -CH_3 groups from *tert*-butyl groups and long carbon chains. Each *tert*-butyl group is involved in seven weak interlayer electrostatic interactions with three different cations (solely -CH_3 groups), two intralayer and two intramolecular interactions (mostly -CH_2 groups).

The hydrogen bond network is significantly extended not at least due to the presence of water. The latter form strong associates with the two neighboring Br^- anions ($d_{H\cdots Br}$ = 2.43−2.47 Å) and accept H-bonds from four neighboring cations, exclusively imidazolium and α methylene hydrogens from the both parts of the bilayer. The architecture of C−H···Br interactions is different also compared to **1** and **3**. Each Br^- anion is connected to four cations with strong preference to one part of the bilayer (~90% in average). These bonds are not restricted to imidazolium and α methylene hydrogens and may include even hydrogens from the first benzene ring and both arms of the same cation. In average C−H···Br contacts in **2** are comparable but the most significant fraction is located around 2.9 Å. Though the water molecule significantly affected the polar part of the structure it is hard to estimate its role in total structural changes in **2**, especially mutual reorientation of the long carbon chains and azobenzene units.

Table 1. Crystallographic and refinement details for compounds **1**, **2**·0.5 H_2O and **3**.

Compound	**1**	**2**·0.5 H_2O	**3**
Substituent	Me	t-Bu	OMe
Empirical	$C_{30}H_{43}N_4OBr$	$C_{33}H_{50}N_4O_{1.5}Br$	$C_{30}H_{43}N_4O_2Br$
CCDC	1902398	1902400	1902399
Formula weight	555.59	606.68	571.59
Space group, *Z*	$P\bar{1}$, 2	*Cc*, 8	$P\bar{1}$, 2
SG No.	2	9	2
a, Å	6.854(5)	52.972(6)	6.8342(1)
b, Å	8.234(6)	8.6963(8)	8.1601(1)
c, Å	27.248(2)	15.054(1)	27.6004(4)
α, °	90.87(9)	90	88.892(2)
β, °	90.87(9)	98.138(3)	89.877(2)
γ, °	109.43(7)	90	69.752(1)
Volume	1449.7(18)	6865.1(9)	1443.81(4)
Temperature [K]	170	293	170
Calculated	1.27	1.174	1.31
Absorption	1.446	1.228	2.192
F(000)	588	2584	604
Θ-range for data	2.6 to 25.00 °	2.3 to 26.8 °	3.2 to 68.0 °
Index ranges	-7 <h< 8	-66 <h< 66	-6 <h< 8
	-9 <k< 9	-11 <k< 11	-9 <k< 9
	-32 <l< 28	-17 <l< 19	-33 <l< 33
Data/	4366/ 325	13651/ 686	5260/ 336
Goodness-of-fit	1.069	0.988	1.129
R_1; ωR_2 [I_0>2σ	0.047; 0.063	0.049; 0.110	0.035; 0.038
R1; ωR2 (all	0.116; 0.129	0.118; 0.135	0.095; 0.096
Flack parameter	–	0.019(12)	–
Largest diff. peak	0.34/ -0.52	0.30/ -0.28	0.75/ -0.51

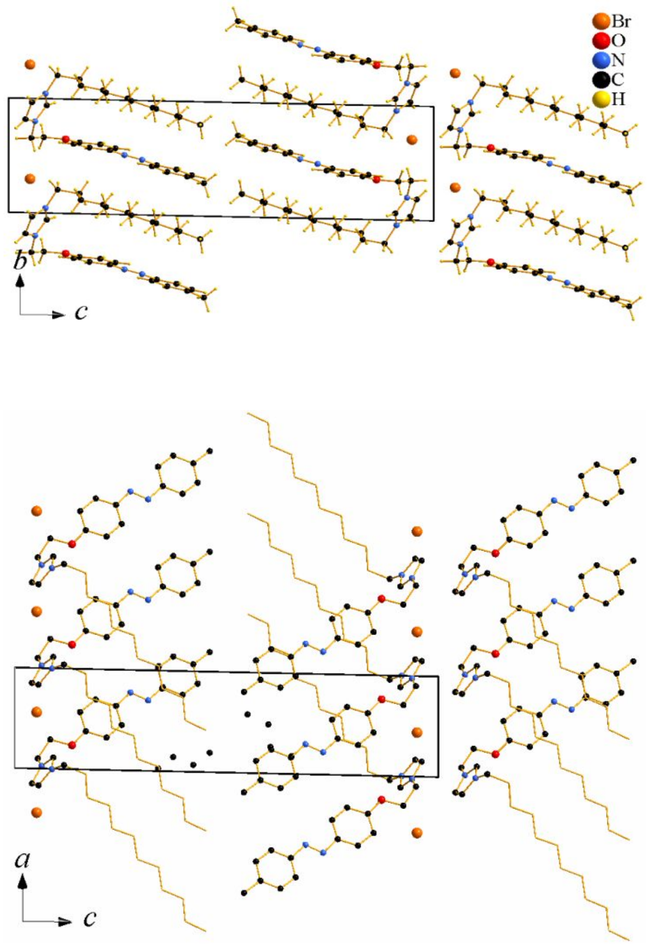

Figure 3. Projections of the crystal structure of compound **1** on the *bc* (top) and the *ac* (bottom) plane.

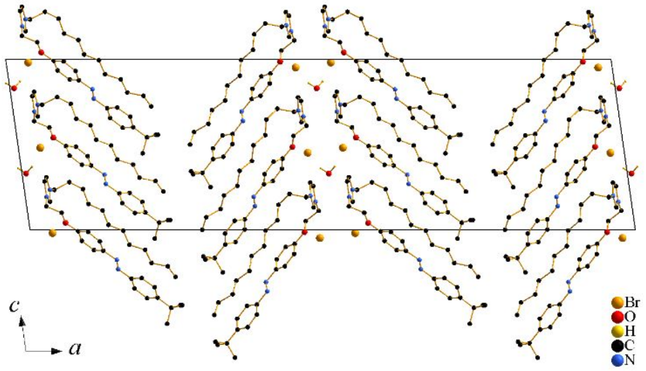

Figure 4. Projections of the crystal structure of compound **2**·0.5 H_2O on the *ac* plane.

3.3. Thermal behavior

The thermal phase behavior of all compounds were examined by polarizing optical microscopy (POM) and differential scanning calorimetry (DSC). The transition temperatures, enthalpies and phase transition assignments are listed in Table 2. The thermal decomposition temperatures and water content were determined *via* thermogravimetric analysis (TGA). All compounds decompose between 250 and 270°C. TGA confirms compounds **1**, **3**, **4** and **5** to be anhydrous and **2** to be a hemihydrate. The second heating and cooling traces for all compounds are displayed in Figure 5. All following heating and cooling cycle show the same thermal events.

Table 2. Thermal properties of compounds **1**–**5.**

			heating[a]		cooling[a]		
No.	**Substituent**	**Transition[b]**	**T [°C]**	**ΔH [kJ/mol]**	**T [°C]**	**ΔH [kJ/mol]**	**T_d[c][°C]**
1	Me	SmA→Cr	63.6	-16.41			
		Cr →SmA	132.9	18.34			263.7

		SmA→L_{ISO}	169.6	2.66	166.9	-2.87	
2	*t*-Bu	SmA →Cr	66.8	-52.60			270.3
		Cr→ SmA	99.5	38.72			
		SmA →L_{ISO}	193.5	3.95	190.6	-4.18	
3	OMe	Cr → L_{ISO}	101.4	21.18			258.4
		L_{ISO}→ SmA			107.4	-2.69	
		SmA → Cr			57.1	-16.32	
4	NMe_2	Cr→ SmA	31.3	12.16	30.4	-12.82	258.3
		SmA →L_{ISO}	89.7	1.27	88.5	-1.52	
5	NO_2	Cr →L_{ISO}	101.7	13.29	77.9	-14.05	256.4

[a] Phase-transition temperatures (°C) and enthalpies are measured during heating and cooling at 5°C/min; [b] the phase transitions were identified by POM measurements; [c] thermal decomposition temperature.

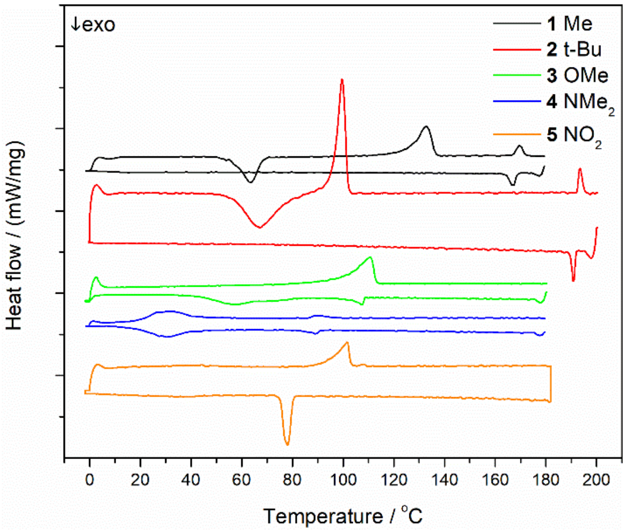

Figure 5. DSC thermogramms of compounds **1**–**5**. For each compound the upper (lower) line corresponds to the 2nd heating (cooling) curve.

Compounds **1** and **2** with methyl and *tert*-butyl (*t*-Bu) substituents, respectively, show one exothermic and two endothermic events during heating (Figure 5). The exothermic event corresponds to a cold crystallization (63.6°C (**1**) and 66.8°C (**2**)). Temperature dependent POM identifies the first endothermic transition (132.9°C/99.5°C) to be the flow point (S→LC) and the second transition (169.6°C/193.5°C) as the clearing point (LC→L_{ISO}). The liquid crystalline phase, which could be identified as a smectic A phase by polarizing microscopy, reappears at 166.9°C (**1**) and 190.6°C (**2**) upon cooling the isotropic liquid. No crystallization occurs during further cooling. Compound **3** melts into an isotropic liquid at 101.4°C without showing other phase transitions. During cooling for **3**, a smectic A phase is formed at 107.4°C. Crystallization occurs upon further cooling at 57.1°C. Compound **4** which features a *N*,*N*-dimethylamino substituent shows two phase transition upon heating as well as upon cooling. It exhibits a smectic A phase around room temperature and clears at 89.7°C. Both transitions are reversible and reappear during cooling, albeit at slightly lower temperatures (Table 2). Compound **5**, where the cation contains a nitro group in *para* position of the azobenzene ring, does not exhibit a mesophase (Figure 5). Upon heating it melts directly into the isotropic liquid at 101.7°C. It recrystallizes during cooling at 77.9°C. Compound **2** (*t*-Bu) has the largest liquid crystalline temperature window:

almost 100°C, while compound **4** (NMe_2) has the lowest flow point (31.3°C) and the lowest clearing point (89.7°C).

Although compounds **1** and **3** have a similar crystal structure (Figure 3), their thermal behavior is entirely different. Compound **3** does not exhibit a mesophase upon heating whereas compound **1**, which shows a cold crystallization upon (re-)heating, forms a liquid crystalline phase over a wide temperature range. It appears, that the additional oxygen atom of the -OMe group is able to efficiently stabilize the crystalline structure and hinders the mesophase formation, probably due to an immobilization of the azogroup. Compound **2** shows a similar thermal behavior to compound **1**, but has a substantially larger mesophase temperature window, in fact the largest amongst all investigated compounds. In contrast, compound **4** has a small mesophase range of 58.4°C. No liquid crystalline phase is formed by compound **5**. The crystal structure of **2** shows that between the layers the substituents are facing each other (Figure 4). Thus, if there are polar groups like in compounds **4** and **5**, repulsive forces are operating that prevent recrystallization. Whereas with aliphatic substituents van der Waals interactions can hold the structure together.

The identification of transition temperatures and proof of mesophase formation was accomplished by POM (polarizing optical microscopy). Figure 6 shows two representative POM textures for observed mesophases obtained by heating and cooling of the compounds. Smectic A phases were recognized by the formation of oily streak or focal conic textures with homeotropic domains (Figure 6).

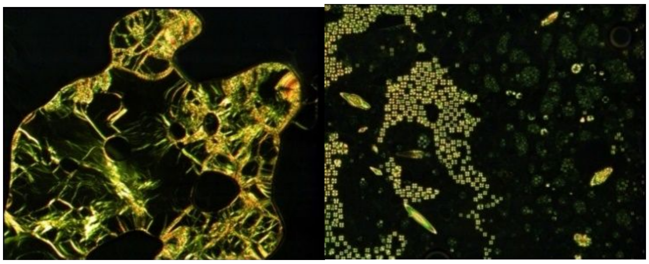

Figure 6. Representative textures as seen between crossed polarizers: (left) oily streak texture of compound **2** at 103.1°C, (right) focal conic texture upon cooling of compound **3** at 107.3°C.

3.4. Photochromic properties

The thermodynamically stable form of compounds **1**–**5** is when they adopt the *trans* conformation. As many other, azobenzene-containing compounds, they can be converted to the *cis* conformation upon irradiation with UV.[57] The photophysical properties of **1**–**5** were studied by transmittance and reflectance UV-Vis spectroscopy. The UV-Vis absorption spectra of methanolic solutions of **1**–**5** are presented in Figure 7 and the relevant numerical data are collected in Table 3. In the spectra of non-irradiated solutions, the strongest absorption band is located in the range of 340–410 nm, while the weakest one is found in the region of 430–440 nm. These bands can be ascribed to the π–π* and *n*–π* transitions of the azobenzene chromophore of the *trans* isomer.[45,58] In the spectrum of **1**, this π–π* band is centered at 343 nm. For comparison, in the spectra of **2**, **3** and **4**, that band is red-shifted by 1, 9 and 65 nm, respectively. Thus, a red-shift with increasing electron-donating ability, with +M-effects having a larger influence than +I-effects, of the substituent occurs, following the order: Me (1) < *t*-Bu (2) < OMe (3) < NMe_2 (4). This observation is in agreement with a reduced HOMO and LUMO gap.[59] On the other hand, almost no shift is observed for the *n*–π* band. For compounds **1**–**4** that weak band appears in the narrow range of 430–435 nm. In the spectra of irradiated solutions, the relative intensities of the π–π* and *n*–π* bands change in such a way that the intensity of the π–π* band decreases, while that of the *n*–π* band increases. However, the π–π* band is still the strongest one. Furthermore, in the spectra of irradiated solutions, the maximum of the π–π* band is blue-shifted by 11 nm for **1**, 40 nm for **2**, 42 nm for **3**, and 28 nm for **5** in comparison with the spectra of non-irradiated solutions. It relates to the fact that when the amount of the *cis* isomer increases, the *π*-conjugation of the azobenzene chromophore decreases. As a consequence, the energy difference between HOMO and LUMO orbitals increases and the blue-shift of the absorption band occurs.[60] On the other hand, the maximum of the *n*–*π** band is red-shifted by 7 nm for **1**, 4 nm for **2**, 12 nm for **3** and 1 nm for **5**. Based on the UV-Vis spectra of solutions of **1**–**3** and **5**, it can be noticed that the greater the blue-shift of the *π*–*π** band after UV irradiation, the more complete the *trans-cis* isomerization. According to that, the highest contribution of *cis* isomer (92%) is found in the solution of **3**, whose spectrum shows the largest blue-shift (42 nm). For comparison, the blue-shift and the contribution of *cis* isomer equal 11 nm and 53% for **1**, 40 nm and 90% for **2**, and 28 nm and 68% for **5**. The methanolic solution of **4** can also exhibit *trans-cis* isomerization. However, the conversion is very limited because of a large overlap of the *π*–*π** and *n*–*π** bands. The irradiation of the solution of **4** at the maximum of the *π*–*π** band (λ = 408 nm) causes the decrease in the intensity of this band due to the formation of the *cis* isomer. Nevertheless, a full conversion cannot be achieved because the reverse reaction is activated as well. In the case of compound **4**

with the *N*,*N*-dimethylamino group only a minor isomerization can be induced due to a strong overlap of the π–π^* and n–π^* bands. Therefore, no spectrum of the solution of **4** with the *cis* isomer is shown here.

The UV-Vis absorption spectra of neat samples of **1**–**5** are presented in Figure 8. Similarly as the spectra of solutions, the spectra of neat samples exhibit bands that can be assigned to the π–π^* and n–π^* transitions of the azobenzene unit. Additionally, these spectra reveal a strong band at around 205 nm that can be attributed to the π–π^* transition of the imidazolium ring. In the case of spectra of solutions, only the right edge of that band is detected above 200 nm. Each sample was once molten before the measurement. Hence, during the measurement, compounds **1**–**4** were in the LC mesophase, while compound **5** was crystalline solid. As a result, if one compares the spectra of non- and irradiated neat samples, the formation of *cis* isomer is more pronounced in the spectra of **1**–**3** than in the spectrum of **5**. In the spectrum of non-irradiated neat sample of **4**, a significant overlap of the π–π^* and n–π^* bands is observed, like in that of methanolic solution.

Table 3. Photochromic properties of methanolic solutions of compounds **1**–**5**.

No.	R	Without irradiation			Upon irradiation at 366 nm				
		$\lambda_{\pi-\pi^*}$/ nm	$A_{\pi-\pi^*}$/ a.u.	$\lambda_{n-\pi^*}$/ nm	$\lambda^*_{\pi-\pi^*}$/ nm	$A^*_{\pi-\pi^*}$/ a.u.	$\lambda^*_{n-\pi^*}$/ nm	ΔA^a/ a.u.	*cis*^{b}/ %
1	Me	343	0.81	430	332	0.38	437	0.43	53
2	t-Bu	344	0.68	435	304	0.07	439	0.61	90
3	OMe	352	0.36	431	310	0.03	443	0.33	92
4	NMe_2	408	0.65	435	–	–	–	–	–
5	NO_2	363	0.50	438	335	0.16	439	0.34	68

^{a} $\Delta A = A_{\pi-\pi^*} - A^*_{\pi-\pi^*}$, ^{b} $cis = (\Delta A/A_{\pi-\pi^*}) \cdot 100\%$ [61], $A_{\pi-\pi^*}$ and $A^*_{\pi-\pi^*}$ correspond to values at $\lambda_{\pi-\pi^*}$

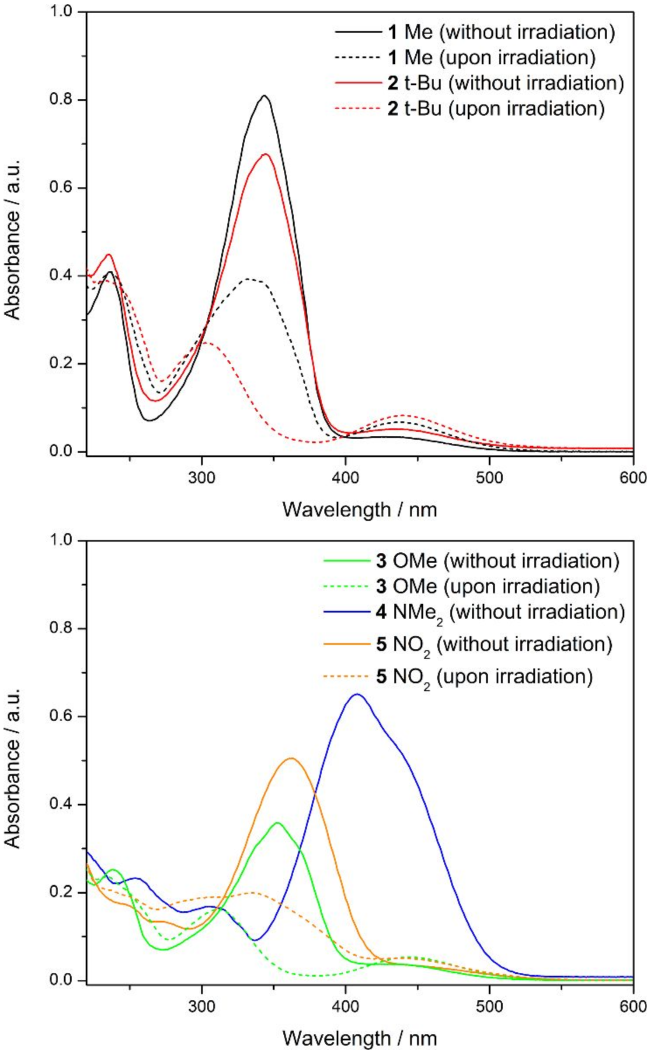

Figure 7. UV-Vis absorption spectra of methanolic solutions of compounds **1**–**5** without and upon irradiation at 366 nm.

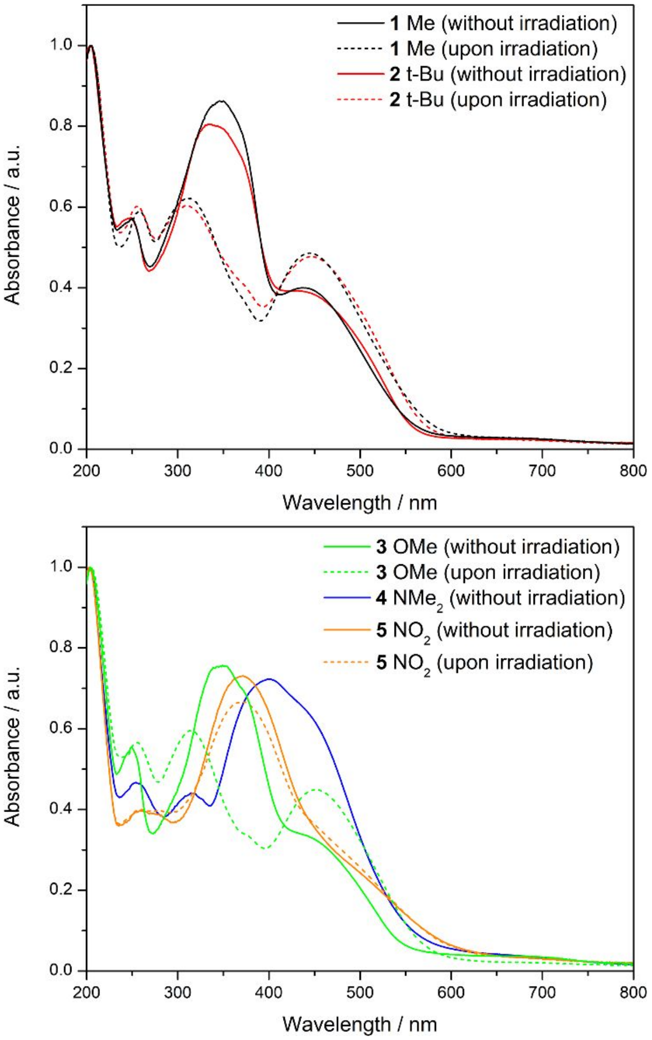

Figure 8. UV-Vis absorption spectra of compounds **1–5** without and upon irradiation at 366 nm.

3.5. The mechanism of photoisomerization and theoretical calculation

The geometries of compounds **1**–**5** in the ground state are first optimized in gas phase. Figure 9 shows 3D-optimized molecular structures of *trans* and *cis* isomers of compound **1**. An intramolecular hydrogen bond is observed between the oxygen and the five-membered ring. Thus, the azobenzene moiety bends towards the five-membered ring. The results of computation reveal that all the *trans* conformations of azobenzene moiety are planar. To further explain the changes of absorption spectrum before and after irradiation, vertical excitation energies and their associated oscillator strengths are obtained using the time dependent density functional theory (TD-DFT) calculations with CAM-B3LYP functionals.[62,63] The highest occupied molecular orbital (HOMO) reflects the ability of the molecule to donate an electron, while lowest unoccupied molecular orbital (LUMO) the ability to receive an electron. The HOMO-LUMO gaps of compounds **1**–**5** are shown in Table 4. The HOMO-LUMO gaps follow the order of Me (**1**) > *t*-Bu (**2**) > OMe (**3**) > NMe_2 (**4**). All figures and energy level diagrams of Molecular Orbitals (MOs) are shown in supporting information. The MOs of *cis* isomers are strongly twisted so that the HOMO energy of *cis* isomer is slightly lower that of *trans* isomer for compounds **1**–**3**. However, with the increase of electron donating ability (compound **4**), the MO shifts away from the substitute group. It leads that the MO of azole bond (HOMO) mainly concentrated on one nitrogen atom, which decreases the conjugation of azole bond. To the contrary, the MO of *cis* isomer of compound **4** does not change significantly with the increase of electron donating ability of the substitute group compared to *trans* isomer since MO on azole bond is conjugated by the lobe on phenyl rings and stabilized by the conjugation. As for LUMO energy, *cis* and *trans* isomers have similar energy. But *cis* isomer is slightly lower than that of *trans* isomer since the twisted structure of azole bond facilitates the overlap of the anti-bonding orbital on phenyl ring and that of azole bond, which is helpful to decrease the energy.

All the simulated absorption spectra are shown in the supporting information. All the simulated maximum absorption bands of *trans* isomers match well with the experimental data. As shown in Figure 10, the oscillator around 430 nm of compound **1** corresponds to an excitation from lone pair electrons of azole bond (*n*-orbital, HOMO-1) to a *π** orbital (LUMO) distributed over the azobenzene moiety, which confirms that the absorption band around 430 nm observed in experiment is *n*–*π** of the azobenzene chromophore of the *trans* isomer. As shown in Figure 11, the oscillator around 340 nm of compound **1** corresponds to the excitation from *π* orbital (HOMO) of azobenzene to *π** orbital (LUMO) of azobenzene. The excitation corresponds to the strongest absorption band in UV-Vis spectroscopy of *trans* isomers. The oscillators and excitation energies of strongest absorption wavelengths are shown in Table 5 for *trans* isomers. It is obvious that the absorption bands are mainly attributed to the excitation from HOMO to LUMO. For *cis* isomers, the contributions of orbitals to absorption bands are complex. Excitations of $S_0 \rightarrow S_1$ and $S_0 \rightarrow S_2$ are shown in Table 6 for reference.

Table 4. HOMO-LUMO gap values of compounds **1–5**.

No.	R	Isomer	HOMO-LUMO gap (eV)	Isomer	HOMO-LUMO gap (eV)
1	Me	*trans*	3.204991	*cis*	2.895837
2	*t*-Bu	*trans*	3.185567	*cis*	2.877061
3	OMe	*trans*	2.885496	*cis*	2.737194
4	NMe_2	*trans*	2.267253	*cis*	2.296642
5	NO_2	*trans*	3.705376	*cis*	3.395983

Table 5. Excitation energies, and oscillator strengths (f) for main absorption band of *trans* isomers of compounds **1**–**5**. Only the maximum wavelengths are shown.

No.	R	Energy (nm/eV)	f	Major contribution
1	Me	340.48/3.6415	1.1702	HOMO→LUMO (96.6%)
		433.84/2.8579	0.0000	HOMO-1→LUMO (94.8%)
2	*t*-Bu	340.74/3.6387	1.2471	HOMO→LUMO (96.6%)
		434.52/2.8533	0.0000	HOMO-1→LUMO (94.7%)
3	MeO	351.72/3.5250	1.2228	HOMO→LUMO (96.7%)
		426.71/2.9056	0.0000	HOMO-1→LUMO (95.0%)
4	NMe_2	392.60/3.1580	1.2991	HOMO→LUMO (95.2%)
		420.88/2.9458	0.0000	HOMO-2→LUMO (94.9%)
5	NO_2	355.36/3.4890	1.2575	HOMO→LUMO (86.1%)
		456.39/2.7166	0.0000	HOMO-1→LUMO (71.2%); HOMO-1→LUMO+1 (24.9%)

Table 6. Excitation energies, and oscillator strengths (f) for main absorption band of *cis* isomers of compounds **1–5**. Only excitations of $S_0 \rightarrow S_1$ and $S_0 \rightarrow S_2$ are shown.

No.	R	Energy (nm/eV)	f	Major contribution
1	Me	293.06/4.2307	0.4384	HOMO-2→LUMO (47.0%)
				HOMO→LUMO (29.1%)
		462.42/2.6812	0.0752	HOMO→LUMO (67.4%)
				HOMO-2→LUMO (18.3%)
2	*t*-Bu	288.17/4.3025	0.3231	HOMO-2→LUMO (27.7%)
				HOMO→LUMO (25.6%)
				HOMO-3→LUMO (18.4%)
				HOMO-1→LUMO (13.0%)
		458.64/2.7033	0.0672	HOMO→LUMO (69.8%)
				HOMO-3→LUMO (11.3%)
3	MeO	292.67/4.2363	0.4270	HOMO-2→LUMO (47.9%)
				HOMO→LUMO (28.4%)
		461.25/2.6880	0.0775	HOMO→LUMO (68.1%)
				HOMO-2→LUMO (17.9%)
4	NMe_2	326.16/3.8013	0.4925	HOMO→LUMO (42.0%)
				HOMO-1→LUMO (29.8%)

				HOMO-2→LUMO (15.7%)
		468.40/2.6470	0.1404	HOMO→LUMO (53.8%)
				HOMO-1→LUMO (23.0%)
				HOMO-2→LUMO (14.3%)
5	NO_2	310.48/3.9933	0.3011	HOMO→LUMO (49.4%)
				HOMO-1→LUMO+1 (23.0%)
		458.27/2.7055	0.0765	HOMO→LUMO (36.4%)
				HOMO→LUMO+1 (30.9%)
				HOMO-1→LUMO+1(10.7%)
				HOMO-1→LUMO (10.1%)

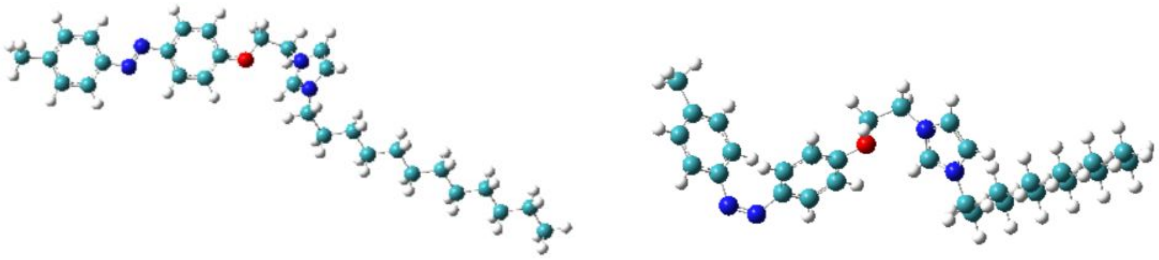
trans *cis*

Figure 9. The optimized 3D molecular structures of *trans* and *cis* isomers of compound **1**.

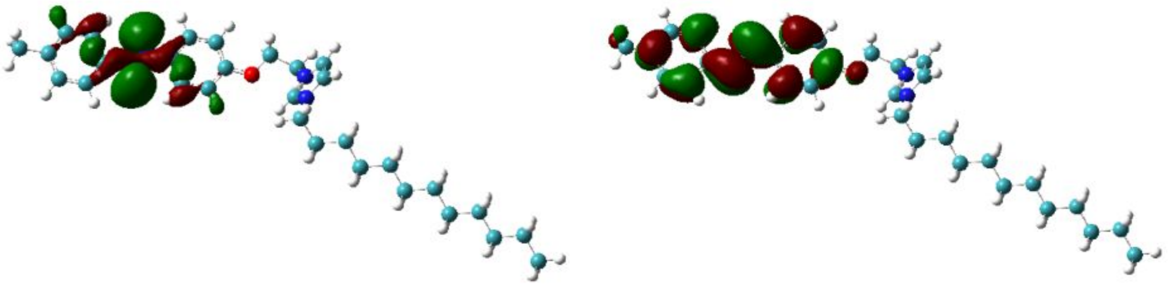

HOMO-1 LUMO

Figure 10. The frontier orbital plots (HOMO-1-LUMO) for optimized geometries of azobenzene derivative compound **1** computed using TD-DFT with functionals of CAM-B3LYP.

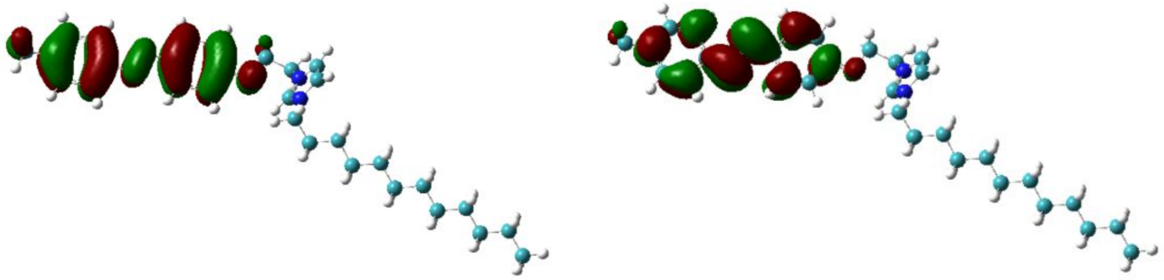

HOMO LUMO

Figure 11. The frontier orbital plots (HOMO-LUMO) for optimized geometries of azobenzene derivative compound **1** computed using TD-DFT with functionals of CAM-B3LYP.

4. Conclusion

A set of five new bromide salts based containing functionalized azobenzene units in the imidazolium cation has been synthesized and characterized. As functional groups methyl-, *tert*-

butyl-, methoxy-, *N*,*N*-dimethylamino and nitro functionalities were investigated, in order to be able to scrutinize structural, steric, and electronic effects. Distinct variations of properties depending on the functional groups can be noted. All compounds melt below 100°C, meeting the formal requirement for the classification as ionic liquids. Four of them are also thermotropic ionic liquid crystals exhibiting smectic A phases. The fifth, bearing nitro group directly melts into an isotropic liquid. From this observation it becomes apparent that directional, specific cation-anion interaction through hydrogen bonding helps to ordering the ions which facilitates the crystallization process. In contrast, the largest mesophase temperature window can be achieved with the hydrophobic, bulky *tert*-butyl group. In addition, crystallization is strongly inhibited as no specific, directional interactions are present and a metastable ionic liquid crystal could be obtained.

The photochromic properties are influenced by the substituents on the azobenzene chromophore as well. An increasing red-shift of the absorption band with the increasing electron-donating character of the substituents. For the *N*,*N*-dimethylamino group substituted compound only a minor isomerization can be induced due to a strong overlap of the π–π* and n–π* bands.

In conclusion, the substitution of different electron donating or withdrawing group on the azobenzene moiety has a substantial influence on the thermal and photoresponse behavior of the ILs. By proper tuning of the electronic levels, i.e. electron donating groups on the azobenzene unit, and avoidance of specific interactions, i.e. directional hydrogen bonding a photoresponsive room temperature ionic liquid crystals could be obtained. This knowledge will help to develop materials for application as sensors and other .

Supporting information

The ^{1}H NMR, ^{13}C NMR, IR, TGA spectra for every compound can be found in the supporting information. The 3D molecular structures and molecular orbitals resulting from the DFT calculations can also be found here.

The Supporting Information is available free of charge on the ACS Publications website.

AUTHOR INFORMATION

Corresponding Author

Anja-Verena Mudring

Email: anja-verena.mudring@mmk.su.se

ORCID

Olivier Renier: 0000-0002-1227-547X

Magdalena Wilk-Kozubek: 0000-0002-1730-0304

Volodymyr Smetana: 0000-0003-0763-1457

Anja-Verena Mudring: 0000-0002-2800-1684

Acknowledgments

A.-V.M. would like to thank the Royal Academy of Sciences, Sweden, for support through the Göran Gustafsson prize in Chemistry, Energimydigheten (The Swedish Energy Agency) for support through grant no. 46676-1 and Stiftelsen för Strategisk Forskning (Swedish Foundation for Strategic Research, SSF) for support in the REFIT research consortium. The Carl Tryggers Foundation (Stockholm, Sweden) is acknowledged by A.-V.M. for a fellowship for M.W.-K.

References

(1) Wasserscheid, P.; Keim, W. Ionic Liquids—New "Solutions" for Transition Metal Catalysis. *Angewandte Chemie* **2000**, *39* (21), 3772–3789.

(2) Wasserscheid, P.; Welton, T. *Ionic Liquids in Synthesis.*; Wiley-VCH: Weinheim, **2007**.

(3) Prodius, D.; Mudring, A.-V. Rare Earth Metal-Containing Ionic Liquids. *Coordination Chemistry Reviews* **2018**, *363*, 1–16.

(4) Morris, R. E. Ionothermal Synthesis—Ionic Liquids as Functional Solvents in the Preparation of Crystalline Materials. *Chemical Communications* **2009**, 21, 2990-2998.

(5) Dupont, J.; de Souza, R. F.; Suarez, P. A. Z. Ionic Liquid (Molten Salt) Phase Organometallic Catalysis. *Chemical Reviews* **2002**, *102* (10), 3667–3692.

(6) Welton, T. Room-Temperature Ionic Liquids. Solvents for Synthesis and Catalysis. *Chemical Reviews* **1999**, *99* (8), 2071–2084.

(7) Revell, J. D.; Ganesan, A. Ionic Liquid Acceleration of Solid-Phase Suzuki−Miyaura Cross-Coupling Reactions. *Organic Letters* **2002**, *4* (18), 3071–3073.

(8) Mehnert, C. P.; Cook, R. A.; Dispenziere, N. C.; Afeworki, M. Supported Ionic Liquid Catalysis − A New Concept for Homogeneous Hydroformylation Catalysis. *Journal of the American Chemical Society* **2002**, *124* (44), 12932–12933.

(9) Shimojo, K.; Kurahashi, K.; Naganawa, H. Extraction Behavior of Lanthanides Using a Diglycolamide Derivative TODGA in Ionic Liquids. *Dalton Transactions* **2008**, 37, 5083-5088.

(10) Wang, J.-H.; Cheng, D.-H.; Chen, X.-W.; Du, Z.; Fang, Z.-L. Direct Extraction of Double-Stranded DNA Into Ionic Liquid 1-Butyl-3-Methylimidazolium Hexafluorophosphate and Its Quantification. *Analytical Chemistry* **2007**, *79* (2), 620–625.

(11) Katsuta, S.; Yoshimoto, Y.; Okai, M.; Takeda, Y.; Bessho, K. Selective Extraction of Palladium and Platinum from Hydrochloric Acid Solutions by Trioctylammonium-Based Mixed Ionic Liquids. *Industrial & Engineering Chemistry Research* **2011**, *50* (22), 12735–12740.

(12) Vander Hoogerstraete, T.; Onghena, B.; Binnemans, K. Homogeneous Liquid–Liquid Extraction of Metal Ions with a Functionalized Ionic Liquid. *The Journal of Physical Chemistry Letters* **2013**, *4* (10), 1659–1663.

(13) Vasudeva Rao, P. R.; Venkatesan, K. A.; Srinivasan, T. G. Studies on Applications of Room Temperature Ionic Liquids. *Progress in Nuclear Energy* **2008**, *50* (2–6), 449–455.

(14) Matsumiya, M.; Suda, S.; Tsunashima, K.; Sugiya, M.; Kishioka, S.; Matsuura, H. Electrochemical Behaviors of Multivalent Complexes in Room Temperature Ionic Liquids Based

on Quaternary Phosphonium Cations. *Journal of Electroanalytical Chemistry* **2008**, *622* (2), 129–135.

(15) O'Mahony, A. M.; Silvester, D. S.; Aldous, L.; Hardacre, C.; Compton, R. G. Effect of Water on the Electrochemical Window and Potential Limits of Room-Temperature Ionic Liquids. *Journal of Chemical & Engineering Data* **2008**, *53* (12), 2884–2891.

(16) *Ionic Liquids*; Kirchner, B., Clare, B., Eds.; Topics in current chemistry; Springer Verlag: Heidelberg ; New York, **2009**.

(17) Weaver, K. D.; Kim, H. J.; Sun, J.; MacFarlane, D. R.; Elliott, G. D. Cyto-Toxicity and Biocompatibility of a Family of Choline Phosphate Ionic Liquids Designed for Pharmaceutical Applications. *Green Chemistry* **2010**, *12* (3), 507-513.

(18) Getsis, A.; Mudring, A.-V. Switchable Green and White Luminescence in Terbium-Based Ionic Liquid Crystals. *European Journal of Inorganic Chemistry* **2011**, *2011* (21), 3207–3213.

(19) Ford, L.; Harjani, J. R.; Atefi, F.; Garcia, M. T.; Singer, R. D.; Scammells, P. J. Further Studies on the Biodegradation of Ionic Liquids. *Green Chemistry* **2010**, *12* (10), 1783-1789.

(20) MacFarlane, D. R.; Kar, M.; Pringle, J. M. *Fundamentals of Ionic Liquids: From Chemistry to Applications*; Wiley-VCH: Weinheim, **2017**.

(21) Stappert, K.; Lipinski, G.; Kopiec, G.; Spielberg, E. T.; Mudring, A.-V. Mesophase Stabilization in Ionic Liquid Crystals through Pairing Equally Shaped Mesogenic Cations and Anions. *Crystal Growth & Design* **2015**, *15* (11), 5388–5396.

(22) Stappert, K.; Ünal, D.; Spielberg, E. T.; Mudring, A.-V. Influence of the Counteranion on the Ability of 1-Dodecyl-3-Methyltriazolium Ionic Liquids to Form Mesophases. *Crystal Growth & Design* **2015**, *15* (2), 752–758.

(23) Aronzon, D.; Levy, E. P.; Collings, P. J.; Chanishvili, A.; Chilaya, G.; Petriashvili, G. Trans–Cis Isomerization of an Azoxybenzene Liquid Crystal. *Liquid Crystals* **2007**, *34* (6), 707–718.

(24) Coleman, S.; Byrne, R.; Alhashimy, N.; Fraser, K. J.; Macfarlane, D. R.; Diamond, D. Photochromic Imidazolium Based Ionic Liquids Based on Spiropyran. *Phys Chem Chem Phys* **2010**, *12* (26), 7009–7017.

(25) Abbaszad Rafi, A.; Hamidi, N.; Bashir-Hashemi, A.; Mahkam, M. Photo-Switchable Nanomechanical Systems Comprising a Nanocontainer (Montmorillonite) and Light-Driven Molecular Jack (Azobenzene-Imidazolium Ionic Liquids) as Drug Delivery Systems; Synthesis, Characterization, and in Vitro Release Studies. *ACS Biomater. Sci. Eng.* **2018**, *4* (1), 184–192.

(26) Forber, C. L.; Kelusky, E. C.; Bunce, N. J.; Zerner, M. C. Electronic Spectra of Cis- and Trans-Azobenzenes: Consequences of Ortho Substitution. *Journal of the American Chemical Society* **1985**, *107* (21), 5884–5890.

(27) Bandara, H. M. D.; Burdette, S. C. Photoisomerization in Different Classes of Azobenzene. *Chem. Soc. Rev.* **2012**, *41* (5), 1809–1825.

(28) Dokić, J.; Gothe, M.; Wirth, J.; Peters, M. V.; Schwarz, J.; Hecht, S.; Saalfrank, P. Quantum Chemical Investigation of Thermal Cis-to-Trans Isomerization of Azobenzene Derivatives: Substituent Effects, Solvent Effects, and Comparison to Experimental Data. *The Journal of Physical Chemistry A* **2009**, *113* (24), 6763–6773.

(29) Nishimura, N.; Kosako, S.; Sueishi, Y. The Thermal Isomerization of Azobenzenes. III. Substituent, Solvent, and Pressure Effects on the Thermal Isomerization of Push-Pull Azobenzenes. *Bulletin of the Chemical Society of Japan* **1984**, *57* (6), 1617–1625.

(30) Cembran, A.; Bernardi, F.; Garavelli, M.; Gagliardi, L.; Orlandi, G. On the Mechanism of the Cis−trans Isomerization in the Lowest Electronic States of Azobenzene: S_0, S_1, and T_1. *Journal of the American Chemical Society* **2004**, *126* (10), 3234–3243.

(31) Saccone, M.; Palacio, F. F.; Cavallo, G.; Dichiarante, V.; Virkki, M.; Terraneo, G.; Priimagi, A.; Metrangolo, P. Photoresponsive Ionic Liquid Crystals Assembled via Halogen Bond: En Route towards Light-Controllable Ion Transporters. *Faraday Discuss.* **2017**, *203* (0), 407–422.

(32) Li, Z.; Yuan, X.; Feng, Y.; Chen, Y.; Zhao, Y.; Wang, H.; Xu, Q.; Wang, J. A Reversible Conductivity Modulation of Azobenzene-Based Ionic Liquids in Aqueous Solutions Using UV/Vis Light. *Phys. Chem. Chem. Phys.* **2018**, *20* (18), 12808–12816.

(33) Tamate, R.; Usui, R.; Hashimoto, K.; Kitazawa, Y.; Kokubo, H.; Watanabe, M. Photo/Thermoresponsive ABC Triblock Copolymer-Based Ion Gels: Photoinduced Structural Transitions. *Soft Matter* **2018**, *14* (45), 9088–9095.

(34) Wang, C.; Hashimoto, K.; Tamate, R.; Kokubo, H.; Morishima, K.; Li, X.; Shibayama, M.; Lu, F.; Nakanishi, T.; Watanabe, M. Viscoelastic Change of Block Copolymer Ion Gels in a Photo-Switchable Azobenzene Ionic Liquid Triggered by Light. *Chem. Commun.* **2019**, *55* (12), 1710–1713.

(35) Ya, Q.; Dong, X.-Z.; Chen, W.-Q.; Duan, X.-M. The Synthesis of Aminoazobenzenes and the Effect of Intermolecular Hydrogen Bonding on Their Photoisomerization. *Dyes and Pigments* **2008**, *79* (2), 159–165.

(36) Natansohn, A.; Rochon, P.; Gosselin, J.; Xie, S. Azo Polymers for Reversible Optical Storage. 1. Poly[4'-[[2-(Acryloyloxy)Ethyl]Ethylamino]-4-Nitroazobenzene]. *Macromolecules* **1992**, *25* (8), 2268–2273.

(37) Ikeda, T.; Tsutsumi, O. Optical Switching and Image Storage by Means of Azobenzene Liquid-Crystal Films. *Science* **1995**, *268* (5219), 1873–1875.

(38) Kim, D. Y.; Tripathy, S. K.; Li, L.; Kumar, J. Laser-induced Holographic Surface Relief Gratings on Nonlinear Optical Polymer Films. *Applied Physics Letters* **1995**, *66* (10), 1166–1168.

(39) Kang, H.-C.; Lee, B. M.; Yoon, J.; Yoon, M. Synthesis and Surface-Active Properties of New Photosensitive Surfactants Containing the Azobenzene Group. *Journal of Colloid and Interface Science* **2000**, *231* (2), 255–264.

(40) Xiao, S.; Lu, X.; Lu, Q.; Su, B. Photosensitive Liquid-Crystalline Supramolecules Self-Assembled from Ionic Liquid Crystal and Polyelectrolyte for Laser-Induced Optical Anisotropy. *Macromolecules* **2008**, *41* (11), 3884–3892.

(41) Wang, C.; Hashimoto, K.; Tamate, R.; Kokubo, H.; Watanabe, M. Controlled Sol–Gel Transitions of a Thermoresponsive Polymer in a Photoswitchable Azobenzene Ionic Liquid as a Molecular Trigger. *Angewandte Chemie International Edition* **2018**, *57* (1), 227–230.

(42) Zhang, Q.; Shan, C.; Wang, X.; Chen, L.; Niu, L.; Chen, B. New Ionic Liquid Crystals Based on Azobenzene Moiety with Two Symmetric Imidazolium Ion Group Substituents. *Liquid Crystals* **2008**, *35* (11), 1299–1305.

(43) Yam, V. W.-W.; Lee, J. K.-W.; Ko, C.-C.; Zhu, N. Photochromic Diarylethene-Containing Ionic Liquids and N-Heterocyclic Carbenes. *Journal of the American Chemical Society* **2009**, *131* (3), 912–913.

(44) Zhang, S.; Liu, S.; Zhang, Q.; Deng, Y. Solvent-Dependent Photoresponsive Conductivity of Azobenzene-Appended Ionic Liquids. *Chemical Communications* **2011**, *47* (23), 6641-6643.

(45) Stappert, K.; Muthmann, J.; Spielberg, E. T.; Mudring, A.-V. Azobenzene-Based Organic Salts with Ionic Liquid and Liquid Crystalline Properties. *Crystal Growth & Design* **2015**, *15* (9), 4701–4712.

(46) Altomare, A.; Cascarano, G.; Giacovazzo, C.; Guagliardi, A. SIR92-A Program for Crystal Structure Solution. *J. Appl. Crystallogr* **1993**, *26*, 343.

(47) Sheldrick, G. M. SHELXT – Integrated Space-Group and Crystal-Structure Determination. *Acta Cryst A* **2015**, *71* (1), 3–8.

(48) Sheldrick, G. M. Crystal Structure Refinement with SHELXL. *Acta Cryst C* **2015**, *71* (1), 3–8.

(49) Stoe&Cie GmbH. *X-RED*; Darstadt, Germany, **2001**.

(50) SAINT, Bruker AXS Inc., Madison, Wisconsin, USA, **2015**.

(51) Stoe, C. X-SHAPE, Version 2.05, Program for Crystal Optimization for Numerical Absorption Correction. *Stoe & Cie GmbH, Darmatadt, Germany* **2004**.

(52) Krause, L.; Herbst-Irmer, R.; Sheldrick, G. M.; Stalke, D. Comparison of Silver and Molybdenum Microfocus X-Ray Sources for Single-Crystal Structure Determination. *J Appl Cryst* **2015**, *48* (1), 3–10.

(53) Brandenburg, K.; Putz, H. DIAMOND: Program for Crystal and Molecular Structure Visualization. *Crystal Impact GbR, Bonn, Germany* **2011**.

(54) Frisch, M. J.; Trucks, G. W.; Schlegel, H. B.; Scuseria, G. E.; Robb, M. A.; Cheeseman, J. R.; Scalmani, G.; Barone, V.; Mennucci, B.; Petersson, G. A. Gaussian 09, Revision B. 01; Wallingford, CT, **2009**.

(55) Perdew, J. P.; Chevary, J. A.; Vosko, S. H.; Jackson, K. A.; Pederson, M. R.; Singh, D. J.; Fiolhais, C. Atoms, Molecules, Solids, and Surfaces: Applications of the Generalized Gradient Approximation for Exchange and Correlation. *Phys. Rev. B* **1992**, *46* (11), 6671–6687.

(56) Tomasi, J.; Mennucci, B.; Cammi, R. Quantum Mechanical Continuum Solvation Models. *Chem. Rev.* **2005**, *105* (8), 2999–3094.

(57) Zhao, Y.; Ikeda, T. *Smart Light-Responsive Materials: Azobenzene-Containing Polymers and Liquid Crystals*; John Wiley & Sons, **2009**.

(58) Birnbaum, P. P.; Linford, J. H.; Style, D. W. G. The Absorption Spectra of Azobenzene and Some Derivatives. *Transactions of the Faraday Society* **1953**, *49*, 735–744.

(59) Bureš, F. Fundamental Aspects of Property Tuning in Push–Pull Molecules. *RSC Advances* **2014**, *4* (102), 58826–58851.

(60) Airinei, A.; Rusu, E.; Barboiu, V. Responsive Behavior of 4-(N-Maleimido) Azobenzene in Polymers with Aromatic Main Chain and Side Chain Linked Units. *Journal of the Brazilian Chemical Society* **2010**, *21* (3), 489–495.

(61) Coelho, P. J.; Castro, M. C. R.; Raposo, M. M. M. Reversible Trans–Cis Photoisomerization of New Pyrrolidene Heterocyclic Imines. *Journal of Photochemistry and Photobiology A: Chemistry* **2013**, *259*, 59–65.

(62) Yanai, T.; Tew, D. P.; Handy, N. C. A New Hybrid Exchange–Correlation Functional Using the Coulomb-Attenuating Method (CAM-B3LYP). *Chemical Physics Letters* **2004**, *393* (1), 51–57.

(63) Peach, M. J. G.; Helgaker, T.; Sałek, P.; Keal, T. W.; Lutnæs, O. B.; Tozer, D. J.; Handy, N. C. Assessment of a Coulomb-Attenuated Exchange–Correlation Energy Functional. *Phys. Chem. Chem. Phys.* **2006**, *8* (5), 558–562.

For Table of Contents only.

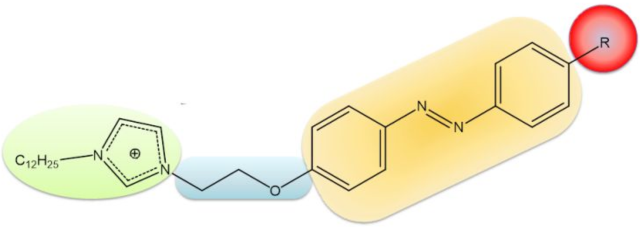

Endowing imidazolium cations commonly used for ionic liquids with mesogenic and photoswitchable units creates an interesting class of soft materials that adopts mesophase structures.